International Journal of Biological Macromolecules 337 (2026) 149592

Contents lists available at ScienceDirect

International Journal of Biological Macromolecules

journal homepage: www.elsevier.com/locate/ijbiomac

Review

The curious life of human mitochondrial SOD2

Medhanjali Dasgupta [a,1], Miles L. Graham [b,1], Gloria E.O. Borgstahl [a,*]

[a] Eppley Institute for Research in Cancer and Allied Diseases, University of Nebraska Medical Center, Omaha, NE, USA
[b] Department of Biochemistry and Molecular Biology, University of Nebraska Medical Center, Omaha, NE, USA

ARTICLE INFO

Keywords:
Manganese superoxide dismutase (MnSOD2)
Iron superoxide dismutase (FeSOD2)
Mitochondrial antioxidants
Redox balance
Oxidative stress
Proton- coupled Electron transfer (PCET)
Metalloenzyme

ABSTRACT

Human manganese superoxide dismutase (MnSOD2) is a critical mitochondrial antioxidant that catalyzes the conversion of highly reactive superoxide radicals into molecular oxygen and hydrogen peroxide. The peroxide molecules are subsequently neutralized by other antioxidant systems, positioning MnSOD2 as the primary defense against mitochondrial oxidative stress and diseases associated with disrupted in vivo redox balance. MnSOD2 has been studied since its discovery in the early 1960s, particularly in the context of cellular pathology and as a therapeutic target. Recent studies combining neutron protein crystallography (NPC), X-ray absorption spectroscopy (XAS), and quantum mechanical (QM) computations have uncovered previously uncharacterized protonation states and atypically short and strong hydrogen bonds within the active site of MnSOD2. Together, these drive the enzyme's exceptionally rapid turnover. This focused review summarizes emerging insights to generate an updated landscape of MnSOD2's structure-function relationship and to highlight remaining challenges. The primary bottleneck to a complete understanding of the structural mechanism of MnSOD2 catalysis is the lack of a superoxide-bound MnSOD2 structure that resolves all proton positions, defines the redox state of the catalytic metal, the metal ligands, and the position of superoxide. Additionally, another largely unexplored area is how Fe substitution converts MnSOD2 into a peroxidase, and how this metal promiscuity affects mitochondrial redox homeostasis. This review synthesizes current evidence and states an informed hypothesis for the catalytic mechanism of Fe-substituted SOD2 (FeSOD2). Clarifying these gaps will advance our understanding of the structural basis of SOD2 catalysis and how it shapes mitochondrial redox biology in health and disease.

1. Introduction

Superoxide radicals ($O_2^{\bullet-}$) are a class of highly reactive oxygen species (ROS), generated as by-products of mitochondrial aerobic respiration, by the one-electron reduction of molecular oxygen (O_2). They accumulate within the mitochondrial matrix because their negative charge from the unpaired electron prevents diffusion across the mitochondrial membrane. Rising levels of the highly reactive nascent $O_2^{\bullet-}$ generate oxidative stress conditions within the mitochondria that negatively impact downstream cell growth and signaling pathways, triggering apoptosis [2–4]. Simultaneously, $O_2^{\bullet-}$ in sub-lethal concentrations acts as a signaling molecule that regulates cellular processes critical for life [5]. Therefore, precisely regulating mitochondrial $O_2^{\bullet-}$ levels by balancing its synthesis and remediation is important because $O_2^{\bullet-}$ imbalance is a key driver of oxidative stress-induced disease pathologies [6]. Such pathologies include: i) chronic inflammation, typically leading to atherosclerosis and type 2 diabetes [7,8]; ii) mitochondrial dysfunction and degeneration, resulting in neurodegenerative disorders such as amyotrophic lateral sclerosis (ALS), cerebral palsy, and Parkinson's disease [9,10]; and iii) impaired metabolic enzymes, DNA damage, unregulated cell growth and proliferation, promoting tumorigenesis, transformation, and metastasis [4,11]. To date, the only known enzyme to successfully remediate $O_2^{\bullet-}$ radicals within the mitochondria is manganese superoxide dismutase (MnSOD2). It dismutes two $O_2^{\bullet-}$ radicals into molecular oxygen (O_2) and hydrogen peroxide (H_2O_2) [12]. These uncharged reaction products are significantly less reactive and can easily diffuse out of the mitochondrial matrix across the membrane, alleviating mitochondrial oxidative stress. This protective role of MnSOD2 against oxidative stress is critical for mitochondrial function, cellular health, and survival, as evidenced by studies that show complete knockout of the SOD2 gene results in early mortality in mice and Drosophila due to reduced activity of several mitochondrial proteins [13–15].

While the MnSOD2-generated H_2O_2 is another class of ROS, it is less

* Corresponding author.
E-mail address: gborgstahl@unmc.edu (G.E.O. Borgstahl).
[1] These authors contributed equally: Medhanjali Dasgupta, Miles L. Graham.

https://doi.org/10.1016/j.ijbiomac.2025.149592
Received 23 October 2025; Received in revised form 26 November 2025; Accepted 8 December 2025
Available online 9 December 2025

damaging than $O_2^{\bullet-}$ and is readily targeted by numerous enzymatic systems, such as peroxidases and catalases, both inside and outside the mitochondria. Interestingly, under certain conditions, including mitochondrial Mn deficiency or Fe enrichment, MnSOD2 readily incorporates Fe into its active site, replacing Mn, to form FeSOD2. FeSOD2 does not dismute $O_2^{\bullet-}$ like its Mn-containing counterpart. Instead, it is a peroxidase [16] [17]. The O_2 generated by MnSOD2 is typically reabsorbed into the mitochondrial electron transfer chain (ETC) for further rounds of aerobic respiration. This review focuses on our current understanding of the structural mechanisms of human MnSOD2 and FeSOD2 enzyme systems.

The physiological form of MnSOD2 is a homotetramer composed of a dimer-of-dimers where subunits A and C form one dimer, and B and D form the other (Fig. 1A) [18]. The tetramer is stabilized by two four-helix bundles that form between the dimers (e.g. A with B and C with D in Fig. 1A), making the tetramer very stable with a Tm of ~88 °C [19]. Each subunit has one active site that contains a metal. Four amino acids, His26, His74, His163, and Asp159, along with a solvent molecule in site-1 (Fig. 1B), directly coordinate the catalytic Mn in a distorted trigonal bipyramidal geometry and are referred to as the inner-sphere residues. The site-1 solvent molecule, typically known as WAT1, is either a water molecule (H2O) in the oxidized form, or a hydroxide ion (OH-) in the reduced enzyme [20–22]. Under certain conditions, a hydroperoxyl anion (HO2-) also binds at site-1 [23]. There are two other solvent binding sites. Site-2 has been observed to contain water molecules or hydrogen peroxide [20,23]. When the inner-sphere site-3 is occupied, the metal geometry becomes octahedral. To date, only inhibitors have been found to bind site-3 (e.g., OH- and Azide) [20,24,25].

MnSOD2 catalyzes the dismutation of two $O_2^{\bullet-}$ radicals into O_2 and H_2O_2 via an extremely fast ($k_{CAT} = 40\ ms^{-1}$; $k_{CAT}/K_m > \sim 10^9\ M^{-1}\ s^{-1}$) (Table 1) two-step ping-pong mechanism [1,18]. The active site metal (Mn) cycles between the oxidized (Mn^{3+}) and reduced (Mn^{2+}) states, as shown below [1,20,26].

$$Mn^{3+}SOD + O_2^{\bullet-} \rightleftharpoons O_2 + Mn^{2+}SOD \quad (k_1 = 1.5\ nM^{-1}s^{-1})$$

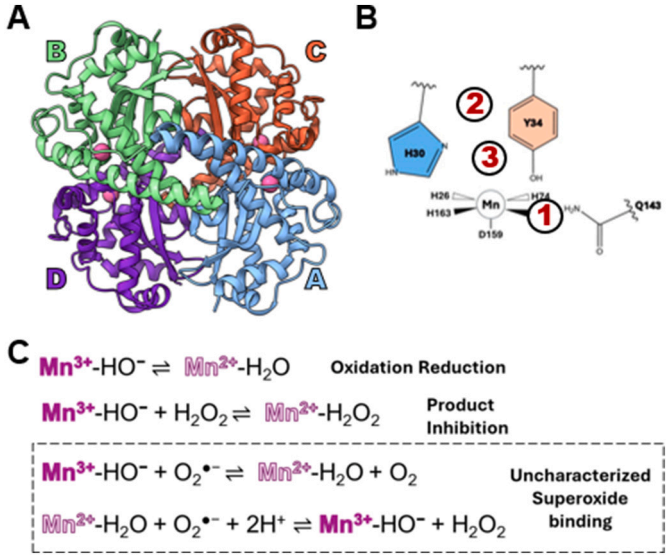

Fig. 1. Structures of MnSOD2. (A) Ribbon diagram of tetrameric resting-state Mn^{3+}SOD; active site Mn ions shown as pink spheres. **(B)** Three solvent ligand binding sites that have been observed to date. Site-1 and site-3 are inner-sphere and site-2 is second sphere. **(C)** The half reactions for solved oxidation-reduction, and peroxide-inhibited structures of MnSOD2. Reactions in the dashed box represent unresolved half-reactions of interest. (For interpretation of the references to colour in this figure legend, the reader is referred to the web version of this article.)

$$Mn^{2+}SOD + O_2^{\bullet-} + 2H^+ \rightleftharpoons H_2O_2 + Mn^{3+}SOD \quad (k_2 = 1.1\ nM^{-1}s^{-1})$$

Catalysis is assisted by the electrostatic guidance of the substrate by residues on the enzyme surface and within the active site funnel [12]. However, there has historically been a significant lack of MnSOD2 structures accurately pinpointing locations of the critical protons that drive the simultaneous proton and electron transfers of the proton-coupled electron transfer (PCET) mechanism of MnSOD2. This hinders a comprehensive understanding of the enzyme's catalytic mechanism.

Recently, the complementary approaches of neutron protein crystallography (NPC) [20,23,27–29], X-ray diffraction (XRD), X-ray absorption spectroscopy (XAS), and Density Functional Theory (DFT) have yielded unprecedented insights into the structural basis of MnSOD2's PCET reaction (Table 2). NPC is particularly attractive for studying metalloenzymes because the neutron beam is chemically inert and does not reduce metals as X-rays do. This method has been indispensable for identifying unusual protonation states of residues and atypical hydrogen bonds within the primary and secondary metal coordination shell in MnSOD2. These unconventional hydrogen bonds are called short strong hydrogen bonds (SSHBs); they are shorter than regular hydrogen bonds, and they form between donor and acceptor groups with similar pK_a values. A low barrier hydrogen bond (LBHB) is a special type of SSHB where the proton is shared equally, and lies midway between donor and acceptor groups [30,31]. Over the last decade, a total of eight NPC structures of oxidized, reduced, product-soaked wild-type (WT), and product-inhibited variants Trp161Phe and Tyr34Phe, have been published, at room and cryogenic temperatures (PDB ID WT: 7KKS, 7KKW; Trp161Phe: 8VHW, 8VHY, 8VJ; Tyr34Phe: 9BVY, 9BW2, 9BWM) [20,23,32]. Combined analysis of these has revealed subtle, but significant reorganization of the network of SSHB and LBHBs in MnSOD2, across redox and product-inhibited states. These hydrogen bond dynamics around the enzyme's active site are important for the proton transfer events driving its PCET.

Moreover, without NPC, it would be impossible to accurately identify the protonation state of the metal-bound solvent at site-1 (H_2O vs OH^- or H_2O_2 vs HO_2^-), resulting in an incomplete picture of this enzyme's active site architecture. In combination with NPC-derived structural information, XAS techniques, such as High Energy Resolution Fluorescence Detected X-ray Absorption Near-Edge Structure (HERFD-XANES) [33,34] and Extended X-ray Absorption Fine Structure (EXAFS) [35], accurately characterize the catalytic metal's electronic state and coordination geometry, as well as, metal-ligand distances. The final data interpretation from the combined analysis is validated to be quantum-mechanically reasonable by performing Density Functional Theory (DFT) calculations [23,36]. More recently, quantum refinement has been used to resolve NPC structures [37]. This integration of complementary methods has fundamentally changed our understanding of the catalytic mechanism of MnSOD2 [20]. Key proton donors driving the PCETs critical for cycling the catalytic Mn during superoxide dismutation were identified, and how product inhibition halts catalysis was revealed [20,23,27–29,32,38].

However, these advances have not yet been comprehensively summarized. This review fills in this gap by providing an integrated perspective on how accurately mapping proton positions in SOD2's active site, coupled with accurate knowledge of catalytic metal electronic states, reveals atypical amino acid ionization and hydrogen bonds, all of which drive SOD2's exceptionally rapid catalysis. Moreover, these approaches validate previously published computational analyses, as well as refine long-standing interpretations of the MnSOD2 product-inhibited complex, to communicate an accurate understanding of the enzyme's structure-function relationship. Additionally, this review investigates how Fe substitution alters the enzyme's activity from a superoxide dismutase to a peroxidase. This helps our understanding of SOD2's mechanistic tuning in response to available metal, as well as the biological consequences of this metal promiscuity. Finally, we highlight critical gaps in current knowledge of the SOD2 enzyme and propose

Table 1
Kinetic parameters for product-inhibited steps of MnSOD2 catalysis.

MnSOD2 Variant	k_{CAT} (ms^{-1})	k_{CAT}/k_m ($\mu M^{-1}\ s^{-1}$)	k_1 ($nM^{-1}\ s^{-1}$)	k_2 ($nM^{-1}\ s^{-1}$)	k_3 ($nM^{-1}\ s^{-1}$)	k_4 (s^{-1})	Gating Ratio (k_2/k_3)
WT	40.0[a]	800.0[a]	1.5[b]	1.1[b]	1.1[b]	120[b]	1
Tyr34Phe[b]	3.3[c]	870.0[c]	0.55[d]	<0.02[d]	0.46[d]	52[d]	<0.04
Trp161Phe[c]	>1[e]	250[e]	0.30[b]	<0.01[b]	0.46[b]	33[b]	<0.02

[a] From Hsu et al. 1996.
[b] From Hearn et al. 2001.
[c] From Guan et al. 1998.
[d] From Greenleaf et al. 2004.
[e] From Cabelli et al. 1999.

Table 2
Complementary experimental techniques and information generated.

Experimental method	Information provided
XRD	Preliminary X-ray structure for NPC data processing pipeline.
NPC	All-atom position, radiation-damage free structure, protonation states of amino acid residues, proton locations, types of hydrogen bonds, and networks.
HERFD-XANES	Metal redox state and electronic configuration.
EXAFS	Metal-ligand distances and coordination geometry.
DFT	Quantum mechanical validation of experimental data.

future directions aimed at resolving these uncertainties, with the goal of fully defining the all-atom catalytic mechanisms of MnSOD2 and FeSOD2 at atomic resolution.

2. Human mitochondrial MnSOD2

The mechanism of MnSOD2's PCET reaction, as well as product inhibition, has long been debated. One of the primary controversies is where superoxide binds MnSOD in the two half reactions. Currently, there are several schools of thought regarding the mechanism:

The "5–6-5" mechanism, proposes that $O_2^{\bullet-}$ binds Mn at the 6th coordination position, opposite Asp159, shifting the pentavalent metal from trigonal bipyramidal to octahedral geometry [39]. Azide (N_3), a potent competitive inhibitor of MnSOD, has been historically used to guide speculations regarding $O_2^{\bullet-}$ binding sites in MnSOD, although the two are significantly different in size and elemental composition. Azide binds the catalytic metal at its vacant, 6th coordination position, opposite the metal-ligated Asp, in *T. thermophilus* MnSOD (PDB ID: 1MNG) and both Mn- and FeSOD isolated from *C. elegans*, via the inner sphere mechanism [12,39–42]. This 6th metal coordination position has also been reported to be occupied by OH^- in *Escherichia coli* MnSOD at pH 8.5 (PDB ID: 1D5N) [25], likely from pH adjustments using hydroxide as a reagent. Recently, Dasgupta and coworkers have reported a partially occupied solvent molecule bound to this 6th Mn-coordination site in the human Gln143Asn MnSOD variant, in both its resting and product-bound states (PDB IDs: 9NR0 and 9NSJ, respectively) [43]. In all these structures, binding of the 6th ligand to the Mn shifts it from its resting state pentavalent distorted trigonal bipyramidal geometry to a hexavalent octahedral geometry.

The "dissociative displacement" mechanism proposes that $O_2^{\bullet-}$ binds Mn at site-1, displacing the bound solvent. In this mechanism, Mn does not undergo any configuration changes, unlike the previous mechanism. This was proposed by Whittaker and Whittaker in *E. coli* MnSOD, at physiological temperature, although they could not verify the identity of the displaced solvent in their studies [44,45]. Interestingly, at lower temperatures, $O_2^{\bullet-}$ binding shifts the pentavalent Mn into octahedral coordination geometry, with an unidentified ligand bound to the 6th position opposite Asp within the inner shell. This was identified as an unstable reaction intermediate, presenting the notion that the binding mechanism of superoxide in MnSOD could be temperature dependent.

Quantum mechanical (QM) studies have predicted that during the first half of the reaction (k_1), $O_2^{\bullet-}$ binds the oxidized metal (Mn^{3+}) via the inner sphere mechanism, while the second $O_2^{\bullet-}$ binds the reduced metal (Mn^{2+}) during the final half (k_2) via the second sphere mechanism [12,32] Interestingly, these QM studies predict no significant difference in activation energy barriers if the second $O_2^{\bullet-}$ binding step occurs via the inner vs the second sphere mechanism, indicating an equal preference of the second $O_2^{\bullet-}$ radical to bind the reduced metal either by directly displacing the site-1 solvent, or by binding the vacant 6th Mn coordination site. The deciding factor appears to be whether or not the second $O_2^{\bullet-}$ radical has space to bind Mn^{2+} in the 6th position [12,32,46,47].

However, the actual substrate binding sites in MnSOD2 remain unsolved, as we currently lack $O_2^{\bullet-}$-bound structures of the enzyme. This is due to experimental challenges posed by the extremely short half-life of $O_2^{\bullet-}$ [48]. This is further discussed in the Conclusions and Perspectives section. The mechanism of MnSOD2 remains unknown, and existing models need to be experimentally verified with $O_2^{\bullet-}$ binding studies.

Another unsolved aspect of the MnSOD2 mechanism is the source and fate of the electron that is transferred to and from the catalytic Mn, driving its redox cycling. It is tempting to speculate that during the first half of the reaction, the incoming $O_2^{\bullet-}$ radical donates its extra electron to the oxidized metal (Mn^{3+}), which then becomes reduced (Mn^{2+}), while the $O_2^{\bullet-}$ is oxidized to the first reaction product, O_2. Computational studies by Noodleman and coworkers [21] proposed that $O_2^{\bullet-}$ cannot immediately donate its extra electron to the oxidized Mn during the first half of the reaction, due to the negative charge on the OH^- anion bound to Mn^{3+} at site-1. These claims, however, remain to be verified experimentally. Recent studies have tested some of the interpretations in the literature with a combination of NPC, XRD, XAS, and DFT techniques (Table 2) [20,23,32].

2.1. Gln143 serves as a proton donor in MnSOD2's PCET reaction

Azadmanesh and coworkers presented experimental evidence that the second-shell residue, Gln143, serves as a critical proton donor in MnSOD2's PCET mechanism [20]. In oxidized Mn^{3+}SOD2, protonated Gln143 forms a hydrogen bond with a OH^- positioned at site 1 (Fig. 2 A-C, Fig. 3 A). Contrastingly, in reduced Mn^{2+}SOD2, a proton is transferred from Gln143 to the site-1 solvent to generate a water molecule, while Gln143 becomes an amide anion (Fig. 2D-F, Fig. 3B). This creates an unusual SSHB between the site-1 bound water and the amide-nitrogen of Gln143($N_{\varepsilon 2}$) in the reduced enzyme. The anionic Gln143 is then stabilized by another SSHB with the proton-donating nitrogen atom of second-sphere residue Trp123($N_{\varepsilon 1}$) (Fig. 2E, Fig. 3A-B). This SSHB lengthens to a regular hydrogen bond in the oxidized enzyme (Fig. 2B, Fig. 3A). Thus, Trp123 plays an indirect role in bolstering MnSOD2 catalysis by stabilizing the anion form of Gln143 in the reduced state. The importance of this hydrogen bonding was noted by Greenleaf and coworkers [49], who observed that the Trp123Phe MnSOD2 variant (PDB 1SZX) had significantly slower kinetics compared to WT MnSOD2 [1,49].

Charge neutralization at the metal center is the key driver of the Gln143 to Mn-bound site-1 solvent PCET event. During the Mn reduction step in the first half of the reaction, the oxidized Mn^{3+} gains an electron

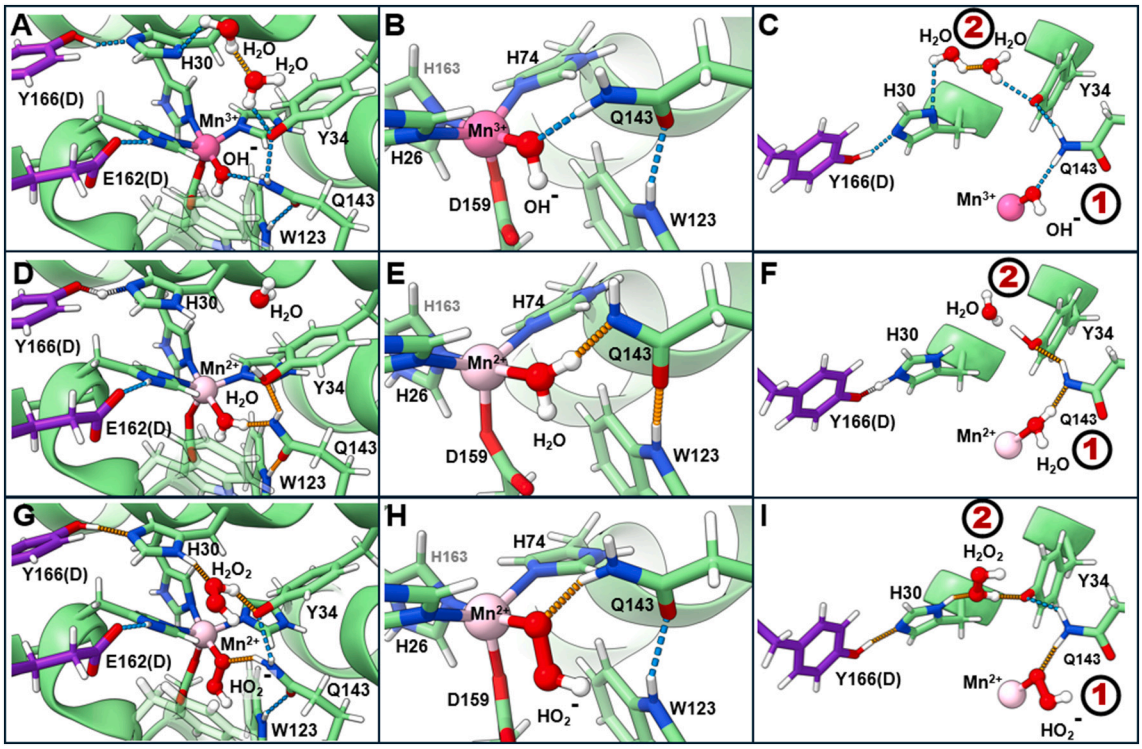

Fig. 2. MnSOD2 active-site hydrogen bonding networks. Panels **(A-C)** show WT oxidized (resting, PDB 7KKS), **(D—F)** WT reduced (PDB 7KKW), and **(G-I)** product-inhibited Trp161Phe MnSOD2 variant (PDB 8VHW), with the Mn^{2+}-bound hydroperoxide ion (HO_2^-) at site 1 and a hydrogen peroxide (H_2O_2) bound between Y34 and H30 in site 2. The oxidized and reduced Mn ions are represented by dark and light pink spheres, respectively. All regular H-bonds are shown as dotted blue lines, and SSHBs are shown as dashed orange lines. The LBHB between H30 and Y166 in the reduced state is shown as dashed white lines **(D & F).** Site-1 and site-2 binding sites are indicated by a red number in a black circle.

Note, careful analysis of WT, Tyr34Phe, and Trp161Phe MnSOD2 by Azadmanesh and coworkers revealed that only chain B of the crystal structures provides an accurate representation of the active site metal coordination environment. In contrast, chain A is often plagued with crystal lattice-induced artefacts and does not always agree with the XAS data. Therefore, the summary of MnSOD2's structural analysis (Figs. 2 and 3), presented in this review, focuses exclusively on chain B. (For interpretation of the references to colour in this figure legend, the reader is referred to the web version of this article.)

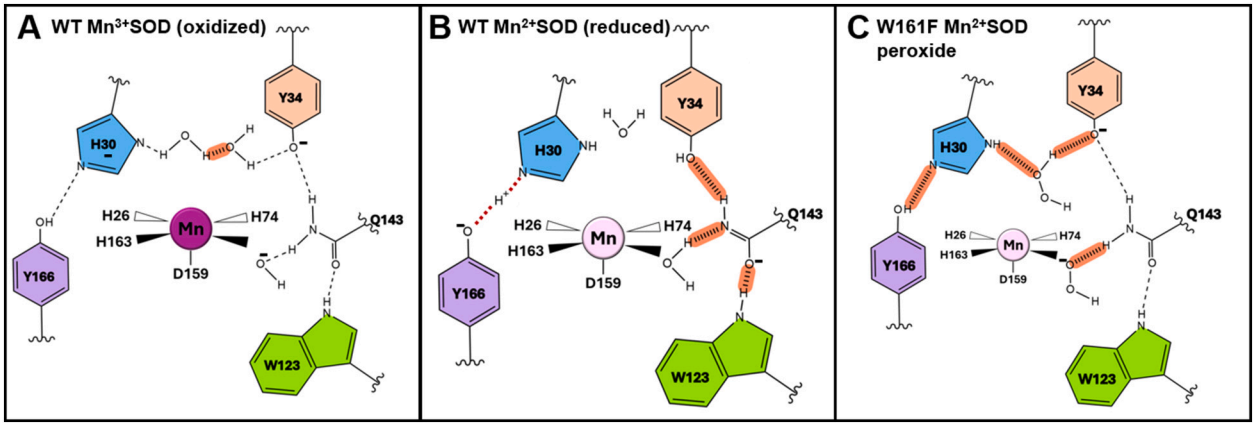

Fig. 3. Active site summaries. Schematic of **(A)** oxidized and **(B)** reduced resting-states of human WT MnSOD2. **(C)** H_2O_2-soaked Trp161Phe MnSOD2. The catalytic Mn in each structure is by a dark pink (for Mn^{3+}) or light pink (for Mn^{2+}) sphere. All SSHBs are represented as orange wide dashed lines, LBHB in the reduced wild-type enzyme is denoted by red dotted line. All regular H-bonds are denoted as black dashed lines. Figure adapted from Azadmanesh et al. 2021 and 2024. (For interpretation of the references to colour in this figure legend, the reader is referred to the web version of this article.)

to generate the reduced Mn^{2+}. This decreases the net positive charge of the metal center and destabilizes active site electrostatics. To compensate, the Mn^{3+}-OH^- is protonated to yield Mn^{2+}-H_2O. In the second half of the reaction, Gln143 regains the proton from Mn^{2+}-H_2O, regenerating the negatively charged OH^- and causing Mn^{2+} to lose the extra electron and become Mn^{3+}, restoring the charge balance at the metal center. Thus, a proton transfer between Gln143 and the Mn-bound site-1 solvent is critical for sustained redox cycling of MnSOD2.

Through this reversible proton transfer event, Gln143 is directly coupled to the redox cycling of the catalytic metal, thus driving catalysis. Substituting Gln143 with Asn preserves the overall backbone architecture but disrupts these critical proton transfer events because Asn143 is positioned too far from the Mn-bound site-1 solvent to effectively participate in proton transfers [50,51]. Consequently, the

resting state of Gln143Asn MnSOD2 is reduced, unlike all other MnSOD2 variants structurally classified so far, and the enzyme has difficulty in redox cycling the Mn. This causes a ~ 130-fold reduction in the kinetic rate constants when Mn^{2+} oxidation to Mn^{3+} is used. This significantly impairs Gln143Asn catalytic turnover (~133-fold decrease in k_{CAT}) [50] relative to WT MnSOD2 (Table 1).

E. coli iron superoxide dismutase (FeSOD) has a conserved Gln69 that is analogous to Gln143 in human MnSOD2. In 2004, Yikilimaz and coworkers [52] demonstrated that the catalytic Fe in FeSOD toggles between the resting-state (oxidized) Fe^{3+}, bound to OH^- at site-1, and a reduced state Fe^{2+} bound to H_2O. The proton transfer event of FeSOD'2 PCET reaction is primarily driven by the second-shell Gln69, in a similar fashion to MnSOD. The authors proposed that Gln69 prefers to stabilize the oxidized state of the enzyme by donating its proton to the site-1 bound solvent, as evidenced by a lowered active site midpoint reduction potential (E_m) in oxidized FeSOD. Replacing Gln69 with Glu substantially elevates the $E_{m,}$ which reflects the variant's preference for the reduced state over the oxidized state, unlike the WT enzyme. Glu69 has an unusual pKa, and is neutral in the oxidized state and ionized in the reduced state, thus participating in PCETs with Fe-ligated solvent. Glu has a canonical pK_a of 4.3, and the pKa of Glu69 in FeSOD must be unusually raised by the proximity to the metal for it to be protonated. Since successful redox cycling of the catalytic metal is a critical determinant of its rate, Gln69Glu FeSOD is catalytically impaired, like the Gln143 Asn MnSOD2 variant. Therefore, second-sphere residues can drastically influence functional properties of metalloenzymes, even without inducing major structural changes.

2.2. Tyr34, His30, and Tyr166 aid MnSOD catalysis by forming a proton transfer wire across the active site gateway

A proton transfer wire connects site-1 to the dimeric interface of MnSOD2 (Figs. 2 and 3). In the oxidized resting state of MnSOD2, the oxygen of Tyr166(O_H) from the adjacent subunit is hydrogen-bonded with His30($N\varepsilon_2$), and, when reduced, this hydrogen bond becomes a LBHB (Fig. 2C,F and Fig. 3B). The significance of this LBHB is highlighted by the reduced catalytic rates observed in His30 variants [53]. Interestingly, in the oxidized enzyme, two water molecules, linked by an SSHB, fully occupy site-2 to bridge the gateway between second-shell residues Tyr34 and His30 (Fig. 2A,C and Fig. 3A). Moreover, in oxidized MnSOD2, both Tyr34 and His30 have unusual pK_a values due to their proximity to the positively charged Mn^{3+}, and at physiological pH their sidechains are deprotonated and negatively charged [20,54]. If their pKas were normal (pKa His = 6.5, pKa = Tyr 10), they would be protonated and neutral at pH 7.8 (the pH of the crystallization condition and pH of mitochondrial matrix). One of the water molecules at site-2 forms a hydrogen bond with Tyr34(O_H), and the other water molecule at site-2 forms a hydrogen bond with His30($N_{\delta1}$). In the reduced state, His30 and Tyr34 are protonated, and only one water molecule is observed at site-2 (Fig. 2D,F and Fig. 3B). The protons for the reduced state water in site-2 are oriented away from His30($N_{\delta1}$) and Tyr34(O_H) and do not form hydrogen bonds with either of them. Thus, in the reduced state, the proton transfer wire is broken at the active site gateway. To connect the wire to the site-1 solvent, Tyr34(O_H) hydrogen bonds with Gln143($N_{\varepsilon2}$), and Gln143($N_{\varepsilon2}$) also hydrogen bonds with the site-1 solvent. These last two hydrogen bonds are normal in oxidized MnSOD2 and SSHBs in reduced MnSOD2 [20]. Overall, in the oxidized resting state of MnSOD2, the wire is composed of regular hydrogen bonds, while in the reduced state, it contains short LBHBs and SSHBs, and the gateway is comparatively more open. During catalytic redox cycling, the active site hydrogen bonds relax and contract like an accordion musical instrument.

These findings reveal how the exceptional catalytic speeds of MnSOD2 (K_{CAT} ~ 40 ms^{-1}) stem from a finely tuned network of unusual hydrogen bonds (SSHBs and LBHBs), as well as unconventional protonation states of key inner- and second-sphere residues owing to the proximity of the positively charged Mn. This understanding offers insights into structural mechanisms that govern rapid, high-efficiency catalysis in metalloenzymes. It is important to note here that the source of this proton transferred through the proton wire remains unknown without solving a $O_2^{\bullet-}$-bound MnSOD2 structure via combined NPC and XAS experiments.

2.3. Product inhibition mechanism of MnSOD2

Human MnSOD2 catalysis can use a slower, product-inhibited pathway that proceeds through the formation, and subsequent rate-limiting resolution of a metal-ligated complex at site-1, typically referred to as the "inhibited complex" (denoted as $Mn^{3+}SOD\text{-}HO_2^-$ below) [26,47,55].

$$Mn^{3+}SOD + O_2^{\bullet-} \rightleftharpoons O_2 + Mn^{2+}SOD \ (k_1 = 1.5\ nM^{-1}s^{-1})$$

$$Mn^{2+}SOD + O_2^{\bullet-} + 2H^+ \rightleftharpoons H_2O_2 + Mn^{3+}SOD \ (k_2 = 1.1\ nM^{-1}s^{-1})$$

$$Mn^{2+}SOD + O_2^{\bullet-} + H^+ \rightleftharpoons [Mn^{3+}SOD - HO_2^-] \ (k_3 = 1.1\ nM^{-1}s^{-1})$$

$$[Mn^{3+}SOD - HO_2^-] + H^+ \rightleftharpoons Mn^{3+}SOD + H_2O_2 \ (k_4 = 120\ nM^{-1}s^{-1})$$

The degree of product inhibition differs between SODs and is quantified by the gating ratio (k_2/k_3) (Table 1) [55–57]. Some SODs, such as *E. coli* and *Deinococcus radiodurans* [58,59], are less affected by product inhibition with gating ratios greater than 1.0 (k_2/k_3 of 4.5 and 16, respectively). WT MnSOD2 has a gating ratio of 1.0 and is susceptible to product inhibition. In this scenario, peroxide release is slowed down by ~110-fold because, rather than direct release during the second half of the MnSOD2 catalytic cycle (k_2), the inhibited complex must resolve the rate-limiting step (k_4). Recent work by Azadmanesh and colleagues has combined NPC and high-resolution XAS techniques to dive deep into the structural and electronic mechanism of product inhibition in MnSOD2 using two highly product-inhibited variants, Tyr34Phe [32] and Trp161Phe [23], with gating ratios of <0.04 and < 0.02, respectively (Table 1) [49,57]. For these variants, the Mn^{2+} to Mn^{3+} half reaction (k_2) is shut down, and the product-inhibited pathway is used 99 % of the time.

Structures of oxidized and reduced Trp161Phe MnSOD2 revealed why this variant is so significantly product-inhibited [23]. They showed two main differences compared to WT: (1) a cavity was created by the mutation near site-1, and (2) the hydrogen bond between Gln143($N_{\varepsilon2}$) and the site-1 solvent was longer and, therefore, weaker. The bond between Mn and O of the site-1 solvent was also longer. These features of the Trp161Phe MnSOD2 variant make it easier for H_2O_2 to displace the site-1 solvent and form the inhibited complex.

The H_2O_2-soaked Trp161Phe MnSOD2 neutron structure [23] shows a hydroperoxyl anion (HO_2^-) bound to the catalytic metal at site-1 to form the inhibited complex (Fig. 2G-I and Fig. 3C). Importantly, XAS data revealed that the metal is reduced in this complex, showing the product-inhibited complex is $Mn^{2+}SOD\text{-}HO_2^-$ and not $Mn^{3+}SOD\text{-}HO_2^-$ as was previously believed. XAS data were critical for correcting this mechanistic aspect of MnSOD2 product inhibition. The neutron structure also showed that site-2 of H_2O_2-soaked Trp161Phe MnSOD2 is occupied by H_2O_2 coordinated with the adjacent de-protonated oxygen of Tyr34 and the protonated $N\delta_1$ of His30 via two SSHBs. This site-2 H_2O_2 binding is in the MnSOD2 gateway to the active site. Importantly, this nuanced distinction between the protonation states of the two di-oxygen species occupying site-1 and site-2 of this variant, i.e., HO_2^- versus H_2O_2, was not possible without NPC.

The Tyr34Phe MnSOD2 variant was also used to study the product inhibited pathway. Comparisons between oxidized and reduced Tyr34-Phe structures and the corresponding WT structures revealed two mutation-induced effects: (1) generation of a cavity near site-1 and site-

2, and (2) removal of the hydrogen bond donor on residue 34. Like in Trp161Phe MnSOD2, the hydrogen bond between Gln143($N_{\varepsilon 2}$) and the site-1 solvent was longer in Tyr34Phe compared to the WT enzyme, but, unlike Trp161Phe, the Mn-site-1 solvent bond lengths were the same as in WT. These features, again, make it easier to form the inhibited complex in Tyr34Phe MnSOD2. The H_2O_2-soaked Tyr34Phe MnSOD2 neutron structure and XAS results [32] revealed a hydroperoxyl anion (HO_2^-) bound to the reduced metal at site-1 to form the inhibited complex, confirming the results observed in product-inhibited Trp161Phe MnSOD2 [23]. Importantly, H_2O_2 binding at site-2 was not observed in the Tyr34Phe variant. Because Tyr34Phe and Trp161Phe MnSOD2 both strongly favor the product-inhibited pathway, it can be concluded that H_2O_2 binding at site-2 is not a critical mechanistic driver of MnSOD2 product inhibition. Site-2 binding of H_2O_2 might account for the even lower gating ratio of Trp161Phe compared to Tyr34Phe MnSOD2 (Table 1).

There is one more observed feature of the product inhibited state. The proton transfer wire in the product inhibited complex is tighter when compared to the oxidized and reduced structures. Four distinct SSHBs form in H_2O_2-treated Trp161Phe MnSOD2, not observed in either oxidized or reduced WT enzyme (Figs. 2 and 3) [20]. SSHBs form between: (1) the deprotonated Tyr34(O_H) and a proton of site-2 H_2O_2, (2) an oxygen of site-2 H_2O_2 and the protonated His30($N_{\delta 1}$), (3) the protonated Tyr166(O_H) and the deprotonated His30($N_{\varepsilon 2}$), and (4) the protonated Gln143($N_{\varepsilon 2}$) and an oxygen of site 2-bound HO_2^-. Only one regular hydrogen bond exists in the product-inhibited wire, and that is between Gln143($N_{\varepsilon 2}$) and Tyr34(O_H). Thus, the hydrogen bonding pattern of the proton transfer wire is different in the product-inhibited complex when compared to the oxidized resting and reduced states. Overall, it is tighter and is an important structural characteristic of the MnSOD2 product-inhibited complex.

3. Human mitochondrial FeSOD2

The SOD2 metal binding site is promiscuous, allowing Fe to replace Mn to form FeSOD2. It is well established that FeSOD2 cannot catalyze $O_2^{\bullet-}$ dismutation and was, therefore, considered catalytically inactive. However, recent discoveries indicate FeSOD2 possesses peroxidase activity [17] (Table 3). This positions FeSOD2 as a powerful prooxidant. FeSOD2 promotes oxidative stress by using H_2O_2 to oxidize various intracellular substrates, an effect exacerbated by correctly metalated MnSOD2, providing a steady supply of H_2O_2 [60] (Fig. 4). Studies have observed FeSOD2 causing oxidative damage in *E. coli* [16] and mitochondrial dysfunction and oxidative stress in mice [61]. H_2O_2 is also membrane diffusible, and its production by MnSOD2 is important for intracellular redox signaling [62]. The presence of FeSOD2 likely disrupts this signaling, possibly attenuating it by consuming H_2O_2 or amplifying it by catalyzing the oxidation of effector redox switches.

Table 3
Comparison of MnSOD2 and FeSOD2. [a]

	Catalytic metal	Enzyme class	Substrate	Products	Biological outcome
MnSOD2	Mn^{3+} Mn^{2+}	Dismutase	$O_2^{\bullet-}$	O_2 H_2O_2	Maintains mitochondrial redox homeostasis by remediating superoxide radicals
FeSOD2	Fe^{4+} Fe^{3+} Fe^{2+}	Peroxidase	H_2O_2 X	H_2O $X^{oxidized}$	Promotes oxidative damage and mitochondrial dysfunction

[a] Where X is an oxidizable biomolecule such as methyl lysine.

Uncovering the exact nature of this disruption requires further study. Reportedly, the in vivo uptake of Fe by SOD2 can be triggered by Mn deficiency or Fe enrichment [61], SOD2 overexpression [16], or SOD2 K68 acetylation [63,64] (Fig. 4). These latter two conditions are implicated in increased tumor malignancy [64–72], implying that FeSOD2 activity plays a role in the tumor-promoting functions of SOD2. FeSOD2's tumor-promoting link is further supported by Bonini and coworkers' recent publication reporting FeSOD2 directly promotes stemness in breast cancer cells by catalyzing H_2O_2-dependent histone demethylation [63]. While surprising that a canonically mitochondrial enzyme could act as a nuclear histone lysine demethylase, it has been shown that there are nuclear SOD2 fractions in bovine pulmonary artery endothelial cells [73] and that oxidative stress triggers nuclear MnSOD2 import in yeast [74]. However, there have been no proposed mechanistic explanations for this metal-dependent shift in activity, nor molecular mechanisms for the peroxidase reaction itself. Overall, the presence of FeSOD2 significantly alters cellular redox homeostasis, leading to disrupted signaling pathways, heightened oxidative stress, and cellular and mitochondrial dysfunction.

As an enzyme, FeSOD2 can be categorized as a mononuclear nonheme Fe enzyme (NHFE). NHFEs catalyze a wide variety of biologically critical functions using a single Fe center to activate a dioxygen species [69]. While most NHFEs use molecular oxygen as their cosubstrate, at least one other NHFE, Fosfomycin-producing Epoxidase (HppE), is reported to use H_2O_2 [70]. Using the proposed HppE mechanism in conjuction with extensive research into NHFE mechanisms by the Solomon group [68,69], we propose a hypothetical mechanism for FeSOD2 below.

$$Fe^{2+} + H_2O_2 \rightarrow O = Fe^{4+} + H_2O$$

$$O = Fe^{4+} + H_2X \rightarrow \left[HO - Fe^{3+} + HX^{\bullet}\right] \rightarrow Fe^{2+} + H_2O + X$$

[Where X is the substrate, such as histone methyl lysine or Amplex Red].

Direct experimental and computational evidence is still needed to confirm this hypothetical mechanism. Future experimental evidence is especially important because FeSOD2 bears key differences compared to other NFHEs that impede direct comparison. Notably

it lacks the "facial triad" (His-X-His-X-Glu/Asp) active site configuration common amongst NHFEs [69] including HppE. Additionally

FeSOD2 distinctively uses only H_2O_2 to catalyze lysine demethylation whereas other NHFEs which perform this reaction require both O_2 and α-ketoglutarate [72]. These properties highlight the need to study the molecular mechanism of FeSOD2 because its elucidation will greatly deepen our understanding of redox biochemistry

4. Conclusions & perspectives

In recent years, significant progress has been made towards a complete understanding of the MnSOD2 catalytic mechanism. However, there are some aspects of this process that remain unknown because of a lack of experimental data. These are discussed below. Ultimately, the application of these methods to the FeSOD2 in a similar fashion would reveal why Fe incorporation fundamentally alters catalysis, changing SOD2 into a peroxidase.

4.1. What does superoxide-bound MnSOD2 look like?

The structure of MnSOD2 bound to its native substrate, $O_2^{\bullet-}$, remains elusive. This gap hinders our understanding of how $O_2^{\bullet-}$ binds to MnSOD2 and the associated structural and electronic changes driving catalysis (Fig. 1C dashed box). Without resolving this, a comprehensive understanding of substrate binding and its role in MnSOD2 catalysis is not possible. However, this understanding is stymied by the two experimental challenges described below.

First, the dismutation reaction is extremely fast. MnSOD2 is one of

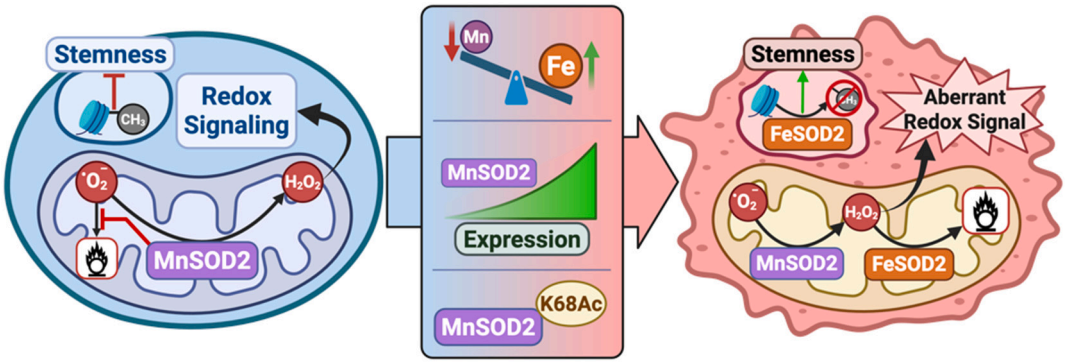

Fig. 4. Overview of the functional relationship between MnSOD2 and FeSOD2, and their effects on the cell. Figure made with BioRender.com.

the fastest known enzymes, causing the development of experimental methods to trap $O_2^{\bullet-}$ transiently-bound to MnSOD2, a significant challenge. One solution is to use a catalytically slow MnSOD2 variant, such as the Gln143Asn [50,51]. This would allow a "slow-motion" version of MnSOD's otherwise rapid catalysis, thus improving the chances of cryo-trapping the elusive substrate-bound MnSOD2 structure. Dasgupta and coworkers solved the structure of H_2O_2 -soaked Gln143Asn MnSOD2 (PDB ID: 9NSJ) [43]. An unprecedented number of peroxide molecules were found trapped outside the active site solvent gateway and extending all the way into the bulk solvent. New product binding sites in MnSOD2 were revealed, adding to the previously identified site-1 and site-2 positions [23,25,32,38]. These results position Gln143Asn MnSOD2 as a viable candidate for superoxide soaking experiments.

Second, there is a lack of methods to soak $O_2^{\bullet-}$ into a protein crystal. Hexagonal MnSOD2 crystals are composed of ~46 % water, presenting a significant challenge when attempting to introduce $O_2^{\bullet-}$ into the protein crystal. This is because, upon contact with water (a proton donor), $O_2^{\bullet-}$ rapidly self-dismutates into O_2 and H_2O_2. The former, being a gas, expands and damages the delicate MnSOD2 crystal lattice, resulting in poor diffraction quality. To date, no method has successfully soaked the native substrate into MnSOD2 crystals. While some studies have investigated the use of aprotic solvents to stabilize $O_2^{\bullet-}$, protein crystals will not survive this treatment [75]. An alternative approach is to generate superoxide in-crystallo by the photolysis of oxygenated formate solution [48].

In conclusion, we summarize recent advances in the structural and mechanistic understanding of MnSOD2, integrating insights from neutron and X-ray protein crystallography with XAS. Overall, a strong understanding of the key mechanistic drivers of MnSOD2 PCET reactions, significantly facilitated by the direct visualization of proton positions from NPC, combined with detailed insights into the catalytic Mn's orbital and ligand coordination geometry from XAS. The same combination of methods could also identify all atom positions in the $O_2^{\bullet-}$ bound active site, filling the last major gap in our knowledge of MnSOD2's activity.

4.2. How does MnSOD2 become a peroxidase?

By incorporating Fe into its active site, MnSOD2 becomes a peroxidase with complete abolishment of its prior dismutase activity. In the absence of any other known changes to the enzyme, it stands that this altered function results solely from the differences in Mn and Fe redox potentials affecting the active site's chemical environment. To achieve an understanding of FeSOD2's mechanism on par with that of MnSOD2, the complementary powers of NPC and XAS can be exploited. NPC enables directly visualizing hydrogen atom positions to discern active site residue and ligand protonation states. This will uncover proton transfer wires facilitating PCETs in FeSOD2's catalytic cycle while identifying critical intermediate Fe-oxygen ligand species. Meanwhile, XAS will elucidate the iron center's electronic environment, uncovering its coordination geometry, molecular orbital configuration, oxidation state, and sub-angstrom ligand distances. Together, these techniques will provide a comprehensive, atomic-level understanding of FeSOD2's active site. It would be of interest to obtain a structural understanding of the binding of substrates (such as H_2O_2 and methyl lysine peptide) to the active site of FeSOD2. Differences observed in the active sites of oxidized, reduced, and ligand-bound FeSOD2, will reveal a step-by-step atomic mechanism for this enigmatic form of SOD2.

An understanding of how metal incorporation alters enzymatic function would be invaluable to the fields of biomimetics and protein engineering. MnSOD2 biomimetic compounds are an attractive avenue for treating diseases caused by oxidative mitochondrial dysfunctions [76]. However, as with MnSOD2 becoming FeSOD2, the possibility may exist for these sorts of MnSOD2 mimics to exhibit metal promiscuity and peroxidase activity. By understanding how FeSOD2 functions on a molecular level, care could be taken in designing biomimetic compounds that are incapable of exhibiting such effects. Conversely, intentionally engineering proteins with peroxidase activity would be made easier. The creation of efficient peroxidase biocatalysts for chemical and pharmaceutical manufacturing, or environmental decontamination are possible applications arising from understanding FeSOD2 activity.

Abbreviations

DFT: Density Functional Theory
EXAFS: Extended X-ray Absorption Fine Structure
HERFD: High Energy Resolution Fluorescence Detected
H_2O: Water
HO_2^-: Hydroperoxyl anion
H_2O_2: Hydrogen peroxidek_{CAT}: Turnover number
HppE: Fosfomycin-producing Epoxidase
k_m: Michaelis constant
LBHB: Low Barrier Hydrogen Bond
Non-heme Fe enzyme (NHFE)
NPC: Neutron Protein Crystallography
OH^-: Hydroxide ion
$O_2^{\bullet-}$: Superoxide
PCET: Proton Coupled Electron Transfer
PDB: Protein Data Bank
SSHB: Short Strong Hydrogen Bond
Tm: Melting temperature
WT: Wildtype
XAS: X-ray Absorption Spectroscopy

CRediT authorship contribution statement

Medhanjali Dasgupta: Writing – review & editing, Writing – original draft, Visualization, Validation, Software, Methodology, Investigation, Formal analysis, Data curation, Conceptualization. **Miles L. Graham:** Writing – review & editing, Writing – original draft,

Visualization, Software, Methodology, Investigation, Formal analysis, Data curation, Conceptualization. **Gloria E.O. Borgstahl:** Writing – review & editing, Supervision, Resources, Project administration, Investigation, Funding acquisition, Formal analysis, Conceptualization.

Declaration of competing interest

The authors declare no competing interests.

Acknowledgements

This work was supported by the NIGMS grant R01-GM145647, the Fred and Pamela Buffett NCI Cancer Center Support Grant (P30CA036727), and Department of Education GAANN fellowship in Structural Biology and Molecular Biophysics (P200A210032). The views expressed here are those of the authors and do not necessarily reflect the official positions of NIGMS or NIH. We thank Dr. Jahaun Azadmanesh and the teams at the Spallation Neutron Source (Oak Ridge National Laboratory, ORNL) and the Stanford Synchrotron Radiation Lightsource (SSRL) for helpful discussions and continued support.

Data availability

No data was used for the research described in the article.

References

[1] R. Bonetta Valentino, The structure-function relationships and physiological roles of MnSOD mutants, Biosci. Rep. 42 (2022) 1–18, https://doi.org/10.1042/BSR20220202.
[2] M. Ott, V. Gogvadze, S. Orrenius, B. Zhivotovsky, Mitochondria, oxidative stress and cell death, Apoptosis 12 (2007) 913–922, https://doi.org/10.1007/s10495-007-0756-2.
[3] I. Martinez-Reyes, J.M. Cuezva, The H(+)-ATP synthase: a gate to ROS-mediated cell death or cell survival, Biochim. Biophys. Acta 1837 (2014) 1099–1112, https://doi.org/10.1016/j.bbabio.2014.03.010.
[4] T.M. Buetler, A. Krauskopf, U.T. Ruegg, Role of superoxide as a signaling molecule, News Physiol. Sci. 19 (2004) 120–123, https://doi.org/10.1152/nips.01514.2003.
[5] J. Checa, J.M. Aran, Reactive oxygen species: drivers of physiological and pathological processes, J. Inflamm. Res. 13 (2020) 1057–1073, https://doi.org/10.2147/JIR.S275595.
[6] J. Grujicic, A.R. Allen, Manganese superoxide dismutase: structure, function, and implications in human disease, Antioxidants (Basel) 14 (2025), https://doi.org/10.3390/antiox14070848.
[7] A. Caturano, M. Rocco, G. Tagliaferri, A. Piacevole, D. Nilo, G. Di Lorenzo, I. Iadicicco, M. Donnarumma, R. Galiero, C. Acierno, C. Sardu, V. Russo, E. Vetrano, C. Conte, R. Marfella, L. Rinaldi, F.C. Sasso, Oxidative stress and cardiovascular complications in type 2 diabetes: from pathophysiology to lifestyle modifications, Antioxidants (Basel) 14 (2025), https://doi.org/10.3390/antiox14010072.
[8] T. Yuan, T. Yang, H. Chen, D. Fu, Y. Hu, J. Wang, Q. Yuan, H. Yu, W. Xu, X. Xie, New insights into oxidative stress and inflammation during diabetes mellitus-accelerated atherosclerosis, Redox Biol. 20 (2019) 247–260, https://doi.org/10.1016/j.redox.2018.09.025.
[9] U.C. Dash, N.K. Bhol, S.K. Swain, R.R. Samal, P.K. Nayak, V. Raina, S.K. Panda, R. G. Kerry, A.K. Duttaroy, A.B. Jena, Oxidative stress and inflammation in the pathogenesis of neurological disorders: mechanisms and implications, Acta Pharm. Sin. B 15 (2025) 15–34, https://doi.org/10.1016/j.apsb.2024.10.004.
[10] C. Guo, L. Sun, X. Chen, D. Zhang, Oxidative stress, mitochondrial damage and neurodegenerative diseases, Neural Regen. Res. 8 (2013) 2003–2014, https://doi.org/10.3969/j.issn.1673-5374.2013.21.009.
[11] N. Hempel, P.M. Carrico, J.A. Melendez, Manganese superoxide dismutase (Sod2) and redox-control of signaling events that drive metastasis, Anti Cancer Agents Med. Chem. 11 (2011) 191–201, https://doi.org/10.2174/187152011795255911.
[12] J. Azadmanesh, G.E.O. Borgstahl, A review of the catalytic mechanism of human manganese superoxide dismutase, Antioxidants (Basel) 7 (2018), https://doi.org/10.3390/antiox7020025.
[13] A. Duttaroy, A. Paul, M. Kundu, A. Belton, A Sod2 null mutation confers severely reduced adult life span in Drosophila, Genetics 165 (2003) 2295–2299, https://doi.org/10.1093/genetics/165.4.2295.
[14] Y.C. Jang, H. Van Remmen, The mitochondrial theory of aging: insight from transgenic and knockout mouse models, Exp. Gerontol. 44 (2009) 256–260, https://doi.org/10.1016/j.exger.2008.12.006.
[15] Y. Li, T.T. Huang, E.J. Carlson, S. Melov, P.C. Ursell, J.L. Olson, L.J. Noble, M. P. Yoshimura, C. Berger, P.H. Chan, D.C. Wallace, C.J. Epstein, Dilated cardiomyopathy and neonatal lethality in mutant mice lacking manganese superoxide dismutase, Nat. Genet. 11 (1995) 376–381, https://doi.org/10.1038/ng1295-376.
[16] D. Ganini, R.M. Petrovich, L.L. Edwards, R.P. Mason, Iron incorporation into MnSOD a (bacterial Mn-dependent superoxide dismutase) leads to the formation of a peroxidase/catalase implicated in oxidative damage to bacteria, Biochim. Biophys. Acta 1850 (2015) 1795–1805, https://doi.org/10.1016/j.bbagen.2015.05.006.
[17] K. Ansenberger-Fricano, D. Ganini, M. Mao, S. Chatterjee, S. Dallas, R.P. Mason, K. Stadler, J.H. Santos, M.G. Bonini, The peroxidase activity of mitochondrial superoxide dismutase, Free Radic. Biol. Med. 54 (2013) 116–124, https://doi.org/10.1016/j.freeradbiomed.2012.08.573.
[18] G.E. Borgstahl, H.E. Parge, M.J. Hickey, W.F. Beyer Jr., R.A. Hallewell, J.A. Tainer, The structure of human mitochondrial manganese superoxide dismutase reveals a novel tetrameric interface of two 4-helix bundles, Cell 71 (1992) 107–118, https://doi.org/10.1016/0092-8674(92)90270-m.
[19] G.E. Borgstahl, H.E. Parge, M.J. Hickey, M.J. Johnson, M. Boissinot, R. A. Hallewell, J.R. Lepock, D.E. Cabelli, J.A. Tainer, Human mitochondrial manganese superoxide dismutase polymorphic variant Ile58Thr reduces activity by destabilizing the tetrameric interface, Biochemistry 35 (1996) 4287–4297, https://doi.org/10.1021/bi951892w.
[20] J. Azadmanesh, W.E. Lutz, L. Coates, K.L. Weiss, G.E.O. Borgstahl, Direct detection of coupled proton and electron transfers in human manganese superoxide dismutase, Nat. Commun. 12 (2021) 2079, https://doi.org/10.1038/s41467-021-22290-1.
[21] W.G. Han, T. Lovell, L. Noodleman, Coupled redox potentials in manganese and iron superoxide dismutases from reaction kinetics and density functional/electrostatics calculations, Inorg. Chem. 41 (2002) 205–218, https://doi.org/10.1021/ic010355z.
[22] J. Heimdal, M. Kaukonen, M. Srnec, L. Rulisek, U. Ryde, Reduction potentials and acidity constants of Mn superoxide dismutase calculated by QM/MM free-energy methods, Chemphyschem 12 (2011) 3337–3347, https://doi.org/10.1002/cphc.201100339.
[23] J. Azadmanesh, K. Slobodnik, L.R. Struble, W.E. Lutz, L. Coates, K.L. Weiss, D.A. A. Myles, T. Kroll, G.E.O. Borgstahl, Revealing the atomic and electronic mechanism of human manganese superoxide dismutase product inhibition, Nat. Commun. 15 (2024) 5973, https://doi.org/10.1038/s41467-024-50260-w.
[24] J. Azadmanesh, S.R. Trickel, G.E.O. Borgstahl, Substrate-analog binding and electrostatic surfaces of human manganese superoxide dismutase, J. Struct. Biol. 199 (2017) 68–75, https://doi.org/10.1016/j.jsb.2017.04.011.
[25] G.E. Borgstahl, M. Pokross, R. Chehab, A. Sekher, E.H. Snell, Cryo-trapping the six-coordinate, distorted-octahedral active site of manganese superoxide dismutase, J. Mol. Biol. 296 (2000) 951–959, https://doi.org/10.1006/jmbi.1999.3506.
[26] I.A. Abreu, D.E. Cabelli, Superoxide dismutases-a review of the metal-associated mechanistic variations, Biochim. Biophys. Acta 2010 (1804) 263–274, https://doi.org/10.1016/j.bbapap.2009.11.005.
[27] J. Azadmanesh, W.E. Lutz, K.L. Weiss, L. Coates, G.E.O. Borgstahl, Redox manipulation of the manganese metal in human manganese superoxide dismutase for neutron diffraction, Acta Crystallogr F Struct Biol Commun 74 (2018) 677–687, https://doi.org/10.1107/S2053230X18011299.
[28] J. Azadmanesh, S.R. Trickel, K.L. Weiss, L. Coates, G.E. Borgstahl, Preliminary neutron diffraction analysis of challenging human manganese superoxide dismutase crystals, Acta Crystallogr F Struct Biol Commun 73 (2017) 235–240, https://doi.org/10.1107/S2053230X17003508.
[29] W.E. Lutz, J. Azadmanesh, J.J. Lovelace, C. Kolar, L. Coates, K.L. Weiss, G.E. O. Borgstahl, Perfect crystals: microgravity capillary counterdiffusion crystallization of human manganese superoxide dismutase for neutron crystallography, NPJ Microgravity 9 (2023) 39, https://doi.org/10.1038/s41526-023-00288-x.
[30] W.W. Cleland, P.A. Frey, J.A. Gerlt, The low barrier hydrogen bond in enzymatic catalysis, J. Biol. Chem. 273 (1998) 25529–25532, https://doi.org/10.1074/jbc.273.40.25529.
[31] J.A. Gerlt, P.G. Gassman, Understanding the rates of certain enzyme-catalyzed reactions: proton abstraction from carbon acids, acyl-transfer reactions, and displacement reactions of phosphodiesters, Biochemistry 32 (1993) 11943–11952, https://doi.org/10.1021/bi00096a001.
[32] J. Azadmanesh, K. Slobodnik, L.R. Struble, J.J. Lovelace, E.A. Cone, M. Dasgupta, W.E. Lutz, S. Kumar, A. Natarajan, L. Coates, K.L. Weiss, D.A.A. Myles, T. Kroll, G. E.O. Borgstahl, The role of Tyr34 in proton coupled electron transfer and product inhibition of manganese superoxide dismutase, Nat. Commun. 16 (2025) 1887, https://doi.org/10.1038/s41467-025-57180-3.
[33] O. Proux, E. Lahera, W. Del Net, I. Kieffer, M. Rovezzi, D. Testemale, M. Irar, S. Thomas, A. Aguilar-Tapia, E.F. Bazarkina, A. Prat, M. Tella, M. Auffan, J. Rose, J. L. Hazemann, High-energy resolution fluorescence detected X-ray absorption spectroscopy: a powerful new structural tool in environmental biogeochemistry sciences, J. Environ. Qual. 46 (2017) 1146–1157, https://doi.org/10.2134/jeq2017.01.0023.
[34] M. Bauer, HERFD-XAS and valence-to-core-XES: new tools to push the limits in research with hard X-rays? Phys. Chem. Chem. Phys. 16 (2014) 13827–13837, https://doi.org/10.1039/c4cp00904e.
[35] J. Li, Y. Li, P.K. Routh, E. Makagon, I. Lubomirsky, A.I. Frenkel, Comparative analysis of XANES and EXAFS for local structural characterization of disordered metal oxides, J. Synchrotron Radiat. 28 (2021) 1511–1517, https://doi.org/10.1107/S1600577521007025.
[36] P. Makkar, N.N. Ghosh, A review on the use of DFT for the prediction of the properties of nanomaterials, RSC Adv. 11 (2021) 27897–27924, https://doi.org/10.1039/d1ra04876g.

[37] K.J.M. Lundgren, O. Caldararu, E. Oksanen, U. Ryde, Quantum refinement in real and reciprocal space using the Phenix and ORCA software, IUCrJ 11 (2024) 921–937, https://doi.org/10.1107/S2052252524008406.
[38] J. Azadmanesh, W.E. Lutz, L. Coates, K.L. Weiss, G.E.O. Borgstahl, Cryotrapping peroxide in the active site of human mitochondrial manganese superoxide dismutase crystals for neutron diffraction, Acta Crystallogr F Struct Biol Commun 78 (2022) 8–16, https://doi.org/10.1107/S2053230X21012413.
[39] M.S. Lah, M.M. Dixon, K.A. Pattridge, W.C. Stallings, J.A. Fee, M.L. Ludwig, Structure-function in Escherichia coli iron superoxide dismutase: comparisons with the manganese enzyme from Thermus thermophilus, Biochemistry 34 (1995) 1646–1660.
[40] G.J. Hunter, C.H. Trinh, R. Bonetta, E.E. Stewart, D.E. Cabelli, T. Hunter, The structure of the Caenorhabditis elegans manganese superoxide dismutase MnSOD-3-azide complex, Protein Sci. 24 (2015) 1777–1788, https://doi.org/10.1002/pro.2768.
[41] M.L. Ludwig, A.L. Metzger, K.A. Pattridge, W.C. Stallings, Manganese superoxide dismutase from Thermus thermophilus. A structural model refined at 1.8 a resolution, J. Mol. Biol. 219 (1991) 335–358.
[42] D.L. Tierney, J.A. Fee, M.L. Ludwig, J.E. Penner-Hahn, X-ray absorption spectroscopy of the iron site in Escherichia coli Fe(III) superoxide dismutase, Biochemistry 34 (1995) 1661–1668.
[43] M. Dasgupta, K. Slobodnik, E.A. Cone, J. Azadmanesh, T. Kroll, G.E.O. Borgstahl, High-resolution X-ray structure of Gln143Asn manganese superoxide dismutase captures multiple hydrogen peroxide-binding sites, Acta Crystallogr F Struct Biol Commun 81 (2025) 467–477, https://doi.org/10.1107/S2053230X25009045.
[44] M.M. Whittaker, J.W. Whittaker, Low-temperature thermochromism marks a change in coordination for the metal ion in manganese superoxide dismutase, Biochemistry 35 (1996) 6762–6770, https://doi.org/10.1021/bi960088m.
[45] M.M. Whittaker, J.W. Whittaker, A "thermophilic shift" in ligand interactions for Thermus thermophilus manganese superoxide dismutase, J. Biol. Inorg. Chem. 2 (1997) 667–671.
[46] M. Srnec, F. Aquilante, U. Ryde, L. Rulisek, Reaction mechanism of manganese superoxide dismutase studied by combined quantum and molecular mechanical calculations and multiconfigurational methods, J. Phys. Chem. B 113 (2009) 6074–6086, https://doi.org/10.1021/jp810247u.
[47] Y. Sheng, I.A. Abreu, D.E. Cabelli, M.J. Maroney, A.F. Miller, M. Teixeira, J. S. Valentine, Superoxide dismutases and superoxide reductases, Chem. Rev. 114 (2014) 3854–3918, https://doi.org/10.1021/cr4005296.
[48] M. Hayyan, M.A. Hashim, I.M. AlNashef, Superoxide ion: generation and chemical implications, Chem. Rev. 116 (2016) 3029–3085, https://doi.org/10.1021/acs.chemrev.5b00407.
[49] W.B. Greenleaf, J.J. Perry, A.S. Hearn, D.E. Cabelli, J.R. Lepock, M.E. Stroupe, J. A. Tainer, H.S. Nick, D.N. Silverman, Role of hydrogen bonding in the active site of human manganese superoxide dismutase, Biochemistry 43 (2004) 7038–7045, https://doi.org/10.1021/bi049888k.
[50] Y. Hsieh, Y. Guan, C. Tu, P.J. Bratt, A. Angerhofer, J.R. Lepock, M.J. Hickey, J. A. Tainer, H.S. Nick, D.N. Silverman, Probing the active site of human manganese superoxide dismutase: the role of glutamine 143, Biochemistry 37 (1998) 4731–4739, https://doi.org/10.1021/bi972395d.
[51] V.J. Leveque, M.E. Stroupe, J.R. Lepock, D.E. Cabelli, J.A. Tainer, H.S. Nick, D. N. Silverman, Multiple replacements of glutamine 143 in human manganese superoxide dismutase: effects on structure, stability, and catalysis, Biochemistry 39 (2000) 7131–7137, https://doi.org/10.1021/bi9929958.
[52] E. Yikilmaz, J. Porta, L.E. Grove, A. Vahedi-Faridi, Y. Bronshteyn, T.C. Brunold, G. E. Borgstahl, A.F. Miller, How can a single second sphere amino acid substitution cause reduction midpoint potential changes of hundreds of millivolts? J. Am. Chem. Soc. 129 (2007) 9927–9940, https://doi.org/10.1021/ja069224t.
[53] C.A. Ramilo, V. Leveque, Y. Guan, J.R. Lepock, J.A. Tainer, H.S. Nick, D. N. Silverman, Interrupting the hydrogen bond network at the active site of human manganese superoxide dismutase, J. Biol. Chem. 274 (1999) 27711–27716, https://doi.org/10.1074/jbc.274.39.27711.
[54] M. Horch, A.F. Pinto, M.A. Mroginski, M. Teixeira, P. Hildebrandt, I. Zebger, Metal-induced histidine deprotonation in biocatalysis? Experimental and theoretical insights into superoxide reductase, RSC Adv. 4 (2014) 54091–54095.
[55] R. Bonetta Valentino, The structure-function relationships and physiological roles of MnSOD mutants, Biosci. Rep. 42 (2022), https://doi.org/10.1042/BSR20220202.
[56] J.J. Perry, A.S. Hearn, D.E. Cabelli, H.S. Nick, J.A. Tainer, D.N. Silverman, Contribution of human manganese superoxide dismutase tyrosine 34 to structure and catalysis, Biochemistry 48 (2009) 3417–3424, https://doi.org/10.1021/bi8023288.
[57] A.S. Hearn, M.E. Stroupe, D.E. Cabelli, J.R. Lepock, J.A. Tainer, H.S. Nick, D. N. Silverman, Kinetic analysis of product inhibition in human manganese superoxide dismutase, Biochemistry 40 (2001) 12051–12058, https://doi.org/10.1021/bi011047f.
[58] I.A. Abreu, A. Hearn, H. An, H.S. Nick, D.N. Silverman, D.E. Cabelli, The kinetic mechanism of manganese-containing superoxide dismutase from Deinococcus radiodurans: a specialized enzyme for the elimination of high superoxide concentrations, Biochemistry 47 (2008) 2350–2356, https://doi.org/10.1021/bi7016206.
[59] J. Zheng, J.F. Domsic, D. Cabelli, R. McKenna, D.N. Silverman, Structural and kinetic study of differences between human and Escherichia coli manganese superoxide dismutases, Biochemistry 46 (2007) 14830–14837, https://doi.org/10.1021/bi7014103.
[60] F.R. Palma, C. He, J.M. Danes, V. Paviani, D.R. Coelho, B.N. Gantner, M.G. Bonini, Mitochondrial superoxide dismutase: what the established, the intriguing, and the novel reveal about a key cellular redox switch, Antioxid. Redox Signal. 32 (2020) 701–714, https://doi.org/10.1089/ars.2019.7962.
[61] D. Ganini, J.H. Santos, M.G. Bonini, R.P. Mason, Switch of mitochondrial superoxide dismutase into a Prooxidant peroxidase in manganese-deficient cells and mice, cell, Chem. Biol. 25 (2018) 413–425 e6, https://doi.org/10.1016/j.chembiol.2018.01.007.
[62] Y. Wang, R. Branicky, A. Noe, S. Hekimi, Superoxide dismutases: dual roles in controlling ROS damage and regulating ROS signaling, J. Cell Biol. 217 (2018) 1915–1928, https://doi.org/10.1083/jcb.201708007.
[63] D.R. Coelho, F.R. Palma, V. Paviani, C. He, J.M. Danes, Y. Huang, J.C.P. Calado, P. C. Hart, C.M. Furdui, L.B. Poole, M.J. Schipma, M.G. Bonini, Nuclear-localized, iron-bound superoxide dismutase-2 antagonizes epithelial lineage programs to promote stemness of breast cancer cells via a histone demethylase activity, Proc. Natl. Acad. Sci. USA 119 (2022) e2110348119, https://doi.org/10.1073/pnas.2110348119.
[64] Y. Zhu, X. Zou, A.E. Dean, J.O. Brien, Y. Gao, E.L. Tran, S.H. Park, G. Liu, M. B. Kieffer, H. Jiang, M.E. Stauffer, R. Hart, S. Quan, K.J.F. Satchell, N. Horikoshi, M. Bonini, D. Gius, Lysine 68 acetylation directs MnSOD as a tetrameric detoxification complex versus a monomeric tumor promoter, Nat. Commun. 10 (2019) 2399, https://doi.org/10.1038/s41467-019-10352-4.
[65] Y. Gao, Y. Zhu, E.L. Tran, V. Tokars, A.E. Dean, S. Quan, D. Gius, MnSOD lysine 68 acetylation leads to cisplatin and doxorubicin resistance due to aberrant mitochondrial metabolism, Int. J. Biol. Sci. 17 (2021) 1203–1216, https://doi.org/10.7150/ijbs.51184.
[66] P.C. Hart, M. Mao, A.L. de Abreu, K. Ansenberger-Fricano, D.N. Ekoue, D. Ganini, A. Kajdacsy-Balla, A.M. Diamond, R.D. Minshall, M.E. Consolaro, J.H. Santos, M. G. Bonini, MnSOD upregulation sustains the Warburg effect via mitochondrial ROS and AMPK-dependent signalling in cancer, Nat. Commun. 6 (2015) 6053, https://doi.org/10.1038/ncomms7053.
[67] C. Zhou, L.H. Lyu, H.K. Miao, T. Bahr, Q.Y. Zhang, T. Liang, H.B. Zhou, G.R. Chen, Y. Bai, Redox regulation by SOD2 modulates colorectal cancer tumorigenesis through AMPK-mediated energy metabolism, Mol. Carcinog. 59 (2020) 545–556, https://doi.org/10.1002/mc.23178.
[68] E.I. Solomon, D.E. DeWeese, J.T. Babicz Jr., Mechanisms of O(2) activation by mononuclear non-Heme Iron enzymes, Biochemistry 60 (2021) 3497–3506, https://doi.org/10.1021/acs.biochem.1c00370.
[69] E.I. Solomon, K.M. Light, L.V. Liu, M. Srnec, S.D. Wong, Geometric and electronic structure contributions to function in non-heme iron enzymes, Acc. Chem. Res. 46 (2013) 2725–2739, https://doi.org/10.1021/ar400149m.
[70] C. Wang, W.C. Chang, Y. Guo, H. Huang, S.C. Peck, M.E. Pandelia, G.M. Lin, H. W. Liu, C. Krebs, J.M. Bollinger Jr., Evidence that the fosfomycin-producing epoxidase, HppE, is a non-heme-iron peroxidase, Science 342 (2013) 991–995, https://doi.org/10.1126/science.1240373.
[71] D. Buongiorno, G.D. Straganz, Structure and function of atypically coordinated enzymatic mononuclear non-heme-Fe(II) centers, Coord. Chem. Rev. 257 (2013) 541–563, https://doi.org/10.1016/j.ccr.2012.04.028.
[72] M.G. Thomas, S.B. Jaber Sathik Rifayee, S.S. Chaturvedi, K.R. Gorantla, W. White, J. Wildey, C.J. Schofield, C.Z. Christov, The unique role of the second coordination sphere to unlock and control catalysis in nonheme Fe(II)/2-oxoglutarate histone demethylase KDM2A, Inorg. Chem. 63 (2024) 10737–10755, https://doi.org/10.1021/acs.inorgchem.4c01365.
[73] S. Zemanovic, M.V. Ivanov, L.V. Ivanova, A. Bhatnagar, T. Michalkiewicz, R. J. Teng, S. Kumar, R. Rathore, K.A. Pritchard Jr., G.G. Konduri, A.J. Afolayan, Dynamic phosphorylation of the C terminus of Hsp70 regulates the mitochondrial import of SOD2 and redox balance, Cell Rep. 25 (2018), https://doi.org/10.1016/j.celrep.2018.11.015, 2605-2616 e7.
[74] S.V. Gupta, L. Campos, K.H. Schmidt, Mitochondrial superoxide dismutase Sod2 suppresses nuclear genome instability during oxidative stress, Genetics 225 (2023), https://doi.org/10.1093/genetics/iyad147.
[75] H. Ukeda, T. Shimamura, M. Tsubouchi, Y. Harada, Y. Nakai, M. Sawamura, Spectrophotometric assay of superoxide anion formed in Maillard reaction based on highly water-soluble tetrazolium salt, Anal. Sci. 18 (2002) 1151–1154, https://doi.org/10.2116/analsci.18.1151.
[76] S. Miriyala, I. Spasojevic, A. Tovmasyan, D. Salvemini, Z. Vujaskovic, D. St Clair, I. Batinic-Haberle, Manganese superoxide dismutase, MnSOD and its mimics, Biochim. Biophys. Acta 1822 (2012) 794–814, https://doi.org/10.1016/j.bbadis.2011.12.002.

Glossary

Gating ratio: The ratio of the rate constants (k_2/k_3) that define how much a SOD uses the product inhibited pathway (larger gating ratios are less effected by product inhibition).

Inner-sphere: In a metalloenzyme, the ligands covalently bound to the catalytic metal within the active site are referred to as the inner-sphere.

Low Barrier Hydrogen Bond (LBHB): A short and strong hydrogen bond formed between a donor and an acceptor group with equal pK_as, where the proton is shared equally and lies midway between both groups. LBHB can be identified using NPC.

Ping-pong Mechanism: A specific type of enzymatic reaction which proceeds via formation of a transient intermediate and allows for one of the reaction products to be released before the second substrate binding events occur.

pK_a: The pK_a value for an amino acid represents the pH at which its functional groups (carboxyl, amino, and side chain) are 50 % ionized and 50 % non-ionized.

Product Inhibition: A phenomenon in which accumulation of excess reaction product inhibits enzymatic activity.

Product Inhibited Pathway: The slower dismutation reaction catalyzed by MnSOD2, which proceeds via the slow resolution of a dead-end kinetic product, prior to product release.

Proton Coupled Electron Transfer: An enzymatic reaction that involves the simultaneous transfer of electrons and protons to generate the reaction end-product(s).

Rate Constant: A measure of an enzyme's catalytic efficiency, measured as the ratio of the concentration of the substrate(s) to that of the product(s), typically denoted by a small k.

Redox signaling: A cellular communication process mediated by the reversible oxidation of signaling transducers by reactive oxygen or nitrogen species

Resting state: The default chemical and electronic state of an enzyme's active site when no substrate is bound and no catalytic turnover is occurring.

Second-sphere: Typically refers to non-covalently bound groups that coordinate with the inner-sphere residues, rather than the catalytic metal, within the active site of a metalloenzyme.

Short Strong Hydrogen Bond (SSHB): A shorter than regular hydrogen bond formed between a donor and an acceptor group with equal pK_as, resulting in strong binding of the donor and the acceptor atoms. An LBHB is a special class of SSHB where the proton is equally shared by the acceptor and donor.

Stemness: Refers to the unique ability of stem cells to differentiate into specialized cell-types.

k_{CAT}*:* Refers to the number of substrate molecules converted into product(s) in unit time when the enzyme is fully saturated with substrate(s).

k_m*:* Refers to the substrate concentration at which an enzyme operates at half of its maximum velocity.

Trigonal bipyramidal geometry: Refers to the three dimensional molecular shape when a central metal atom is covalently bonded to five other atoms or groups, with three arranged in an equatorial triangular plane and the remaining two positioned axially above and below it.

Octahedral geometry: Refers to the three-dimensional molecular shape where a central metal atom covalently binds six atoms or groups arranged at the corners of an octahedron, with 90° bond angles between them.